Indian Journal of Pure & Applied Physics
Vol. 52, December 2014, pp. 829-838

Effect of MoO_3 in the cathode buffer layer on the behaviour of layered organic solar cells

K El Assad Zemallach Ouari[1], Z El Jouad[2,5], K Benchouk[1], B Kouskoussa[1], L Cattin[3], M Makha[2,5], A Khelil[1], M Morsli[4], M Addou[5] & J C Bernède[2]*

[1]LPCMME, Faculté des Sciences, Université d'Oran Es-Sénia, 31100, Oran, Algérie

[2]L'UNAM, Université de Nantes, MOLTECH-Anjou, CNRS, UMR 6200, 2 rue de la Houssinière, BP 92208, Nantes, F-44000 France

[3]Université de Nantes, Institut des Matériaux Jean Rouxel (IMN), CNRS, UMR 6502, 2 rue de la Houssinière, BP 32229, 44322 Nantes cedex 3, France

[4]L'UNAM, Université de Nantes, Faculté des Sciences et des Techniques, 2 rue de la Houssinière, BP 92208, Nantes, F-44000 France

[5]Laboratoire Optoélectronique et Physico-chimie des Matériaux, Université Ibn Tofail, Faculté des Sciences BP 133 Kenitra 14000, Morocco

E-mail: jean-christian.bernede@univ-nantes.fr

Received 1 August 2014; revised 10 October 2014; accepted 10 November 2014

The behaviour of small-molecule organic solar cells based on copper-phthalocyanine/fullerene with different cathode buffer layer is investigated as a function of air exposure duration. The effect of MoO_3 on the properties of photovoltaic solar cells (OPVCs) when it is introduced in the cathode buffer layer (CBL), has been studied. Photovoltaic performances were measured as a function of time of air exposure. During the first days of air exposure, the efficiency of the OPVCs with MoO_3 in their CBL increases significantly, while it decreases immediately after air exposure in the case of reference OPVCs, i.e. without MoO_3 in the CBL. Nevertheless, the lifetime of the OPVCs with MoO_3 in their CBL is around 60 days, while it is only 10 days in the case of reference OPVCs. The initial increase of the OPVC with MoO_3 in their CBL is attributed to the slow decrease of the work function of MoO_3 due to progressive contamination. Then, the progressive degradation of the OPVCs efficiency is due to water vapour and oxygen contamination of the organic layers. The use of double CBL, Alq_3/MoO_3, allows to interrupt the growth of pinholes, defects and increases the path of permeating gas. Also it can prevent the contamination of the organic layer by Al. All this results in significant increase of the lifetime of the OPVCs.

Keywords: Interfaces, Organic compounds, Oxides, Vacuum deposition, Ageing, Electrical properties

1 Introduction

Organic solar cells have the potential advantages of light weight and flexibility. However, not only the power conversion efficiency[1,2] of these cells should be improved, but also their lifetime is far from satisfactory[3-6].The most important degradation causes are photodegradation and environmental parameters. The small molecules, such as copper-phthalocyanines used in our layered organic solar cells, exhibit good photostability and therefore, the lifetime of these cells is mainly dependant on their environment. The important environmental parameters that influence the lifetime of organic solar cells are the diffusion of oxygen and water into the active layers of the cells through the top electrode. The solution to the problem of contaminant diffusion into the active organic layers is the use of barrier layers with low oxygen and water permeability. These layers can be either passive encapsulating layers or a layer present in the solar cell itself such as a cathode buffer layer, or both.

Otherwise, it is known that significant efficiency improvements of layered cells, based on an electron donor/electron acceptor junction, are achieved through the introduction of buffer layers at the interfaces electrodes/organic materials. At the interface electron acceptor/cathode it is assumed that the cathode buffer layer (CBL) allows blocking the excitons[7].

At the interface anode/organic material, it is assumed that the introduction of an anode buffer layer (ABL) allows improving the band matching, and therefore the hole collection, between the anode and

the electron donor. If the PEDOT:PSS was often used, it is not stable[8], so many others materials[9] were probed such as CuI, MoO_3 which is far more stable[8].

More recently, it was proposed to use MoO_3 as cathode buffer layer. As a matter of fact, it is now well accepted that its band gap is around 3.1 eV and that it is *n*-type material. However, the values of its ionization potential (IP), its electronic affinity (χ) and its Fermi level (Wf) are still under discussion. Recently, it was shown that these values measured *in-situ* by ultraviolet photoelectron spectroscopy (UPS) after deposition in ultra high vacuum[10] are IP = 9.7 eV, χ = 6.7 eV and Wf = 6.9 eV. Due to the high values of IP energy of the MoO_3 any hole transport via the valence band is prohibited, while the energy alignment between the band conduction minimum, BC, of MoO_3 and the HOMO of the organic material is favourable for electron transfer between the two materials. From this discussion, MoO_3 can be considered[11,12] for use as CBL.

In the present work, we have investigated this proposition by introducing a thin MoO_3 layer in the CBL of planar OPVCs based on the heterojunction copper phthalocyanine (CuPc)/fullerene (C_{60}). If our study shows that, whatever the thickness of the MoO_3 in the CBL, it induces a decrease of the performance of the OPVC just after realization, it also shows that the efficiency of these OPVCs increases significantly during the first days of air exposure, which results in better efficiency after one week. Then, the variation of the performance of the OPVCs with time is explained by the effect of air contamination which modifies the properties of the interfaces. An electronic modeling is used to comfort the description of the effect of air on devices performances.

2 Experimental Details

The process used for the realization of the OPVCs has been described in Ref. (13).

The CuPc/C_{60} junctions were fabricated on pre-cleaned glass substrate coated with transparent conductive indium tin oxide (ITO) anode. Before organic deposition under vacuum, the ITO substrate was covered with thin MoO_3 layer (3 nm). It was already shown that this layer increases significantly the cells efficiency through a good matching of the band structure [10,13] anode/CuPc. All the different films were deposited in the same run in a vacuum of 10^{-4} Pa. The thin film deposition rate and thickness were estimated *in situ* with a quartz monitor. The deposition rate and final thickness were 0.05 nm/s and 35 nm in the case of CuPc, 0.05 nm/s and.40 nm in the case of C_{60}. The material used as CBL was the aluminium tris(8-hydroxyquinoline) (Alq_3), which is known to be very efficient[14]. In the present work, we added to Alq_3 a MoO_3 layer, the total thickness of the cathode buffer layer being equal to 9 nm as usual[15].

After CBL deposition, the aluminium top electrodes were thermally evaporated, without breaking the vacuum, through a mask with 2 mm × 10 mm active areas. Without protecting layer, the instability of solar cells causes rapid degradation of their performances, the non-encapsulated devices are practically dead after one day in air[16]. In order to mitigate this instability, before breaking the vacuum, an approximately 50 nm encapsulating layer of amorphous selenium (Se-a), is thermally evaporated onto the OPVCs. The selenium protective coating layer (P_{Se}) has been proved to be efficient to protect the under layers from oxygen and water vapour contamination[17], at least during the first hours of room air exposure[16,18]. Encapsulation impedes the process, but does not remove the degradation process. Therefore, the protective layer, increasing the solar cells lifetime, allows improving the duration of the degradation process and therefore, the precision of the study of the EBL effect on this process in order to discriminate between the different contaminants. Finally, the structures used were: glass/ITO(100 nm)/MoO_3(3 nm)/CuPc(35 nm)/C_{60}(40 nm)/EBL(9 nm)/Al(120 nm)/P_{Se}.

Electrical characterizations were performed with an automated I-V tester, in the dark and under sun global AM 1.5 simulated solar illumination. Performances of photovoltaic cells were measured using a calibrated solar simulator (Oriel 300 W) at 100 mW/cm^2 light intensity adjusted with a PV reference cell (0.5 cm^2 CIGS solar cell, calibrated at NREL, USA). Measurements were performed at an ambient atmosphere. All devices were illuminated through TCO electrodes.

Following the protocol proposed in Ref. (3), the procedure used to study the ageing process of our OPVCs corresponds to the intermediate level labelled ''Level 2''.

That is to say, for ageing measurements in air, the samples were stored in the room, in the light of day at open circuit voltage between the measurements. The OPVCs characteristics, the open circuit voltage V_{oc}, the short circuit current density J_{sc}, the fill factor FF and the efficiency η, were studied as follows: multiple tests under AM1.5 light at room temperature were

achieved at different time: 5 min to 2 months. The effect of humidity on the degradation rate of the devices was studied using different storage conditions for samples. Between each J-V characteristic measurements, some samples were placed in closed box with desiccators inside, what resulted in 25% humidity, while others were kept in room air where the humidity was 60%. The humidity was measured by RH88 Humidity transmitter. The temperature of the room was 20°C.

Device lifetime may be defined as the operational lifetime until the performance has fallen below a certain level. In the present case, we choose to use the half-life or decay to 50% performance as a measure of the device lifetime[19] ($T\eta_0/2$).

3 Experimental Results

The evolution with time of the J-V characteristics of the different OPVCs families is shown in Figs 1 and 2 for two typical OPVCs, one with Alq_3 (6 nm)/ MoO_3 (3 nm) as CBL (Fig. 1) and the other one, that we call reference, with 9 nm of Alq_3 as CBL (Fig. 2). The results obtained with the different Alq_3/MoO_3 combinations after different durations, *t*, of air exposure are reported in Table 1. It can be seen that when the CBL contains MoO_3, the efficiency increases during the first days of air exposure up to a value slightly smaller than 1% (Fig. 1, Table 1), while in the case of reference Alq_3 CBL the efficiency is maximum, slightly higher than 1%, for $t = 0$ and then it decreases (Fig. 2). Moreover, when the efficiency of the OPVCs with MoO_3 in their CBL is optimum, i.e. after some days of air exposure, it is superior to that of reference OPVCs for the same exposure time to air. Then, even if the efficiency of all the OPVCs decreases, those with MoO_3 in their CBL stay higher (Fig. 3).

As a matter of fact, if after they have reached their maximum performance thereof decreases quite rapidly for a few days, it then tends to stabilize whereby the lifetime of these cells is of the order of nearly 60 days, while it is only 10 days with reference OPVCs (Fig. 3). About the shape of the J-V characteristics, it can be seen in Figs 1 and 2 that, whatever the kind of CBL used, it varies with the time of air exposure with disappearance / appearance of S-shaped curve. This evolution will be discussed with the help of different electrical schemes.

All the photovoltaic characteristics are normalised to their maximum value and plotted as a function of exposure time to air in Figs 3 and 4.

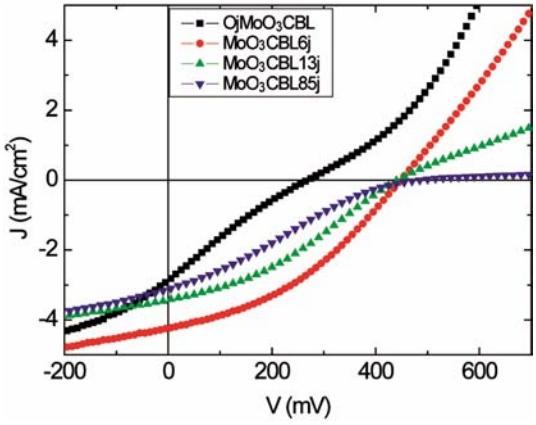

Fig. 1 — J-V characteristics of ITO (100nm)/MoO_3 (3 nm)/CuPc (35 nm)/C_{60} (40 nm)/Alq_3 (6 nm)/MoO_3 (3 nm)/Al OPVC after different durations, t, of air exposure: (■) t = 0, (●) t = 6 days, (▲) t = 13 days and (▼) t = 85 days

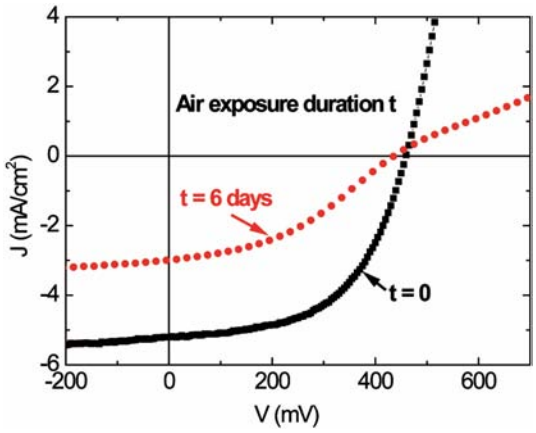

Fig. 2 — J-V characteristics of ITO (100nm)/MoO_3 (3 nm)/CuPc (35 nm)/C_{60} (40 nm)/Alq_3 (9 nm)/Al OPVC after different durations, t, of air exposure: (■) t = 0 and (●) t = 6 days

Normalized η versus time curves for cells stored in ambient atmosphere (Fig. 3) show that the rate of decrease of η depends on the nature of the CBL. Thus, while in a first step all the OPVCs show nearly similar degradation rates, the degradation rate is significantly larger in a second step for reference cells. Moreover, it must be noted that, as the performance of the reference OPVC decreases as soon as their completion, while it decreases only after reaching its maximum, that is to say after several days in the case of cells containing MoO_3 in their CBL, when the slope of the curves of Fig. 3 changes, the efficiency of reference OPVC is much lower. Since devices differ only by the nature of the buffer layers

Table 1 — Evolution with the time of air exposure of the typical parameters of OPVCs with different cathode buffer layer configurations

CBL	*t* (Air exposure in days)	*J*sc (mA/cm^2)	*V*oc (V)	FF (%)	η (%)
	0	0.13	0.011	24	3.7×10^{-4}
Alq_3(3 nm)/ MoO_3(6 nm)	6	4.65	0.47	36	0.80
	10	3.92	0.44	30.5	0.53
	0	2.86	0.27	22	0.17
Alq_3(6 nm)/ MoO_3(3 nm)	6	4.73	0.49	37	0.85
	10	4.13	0.46	35.5	0.67

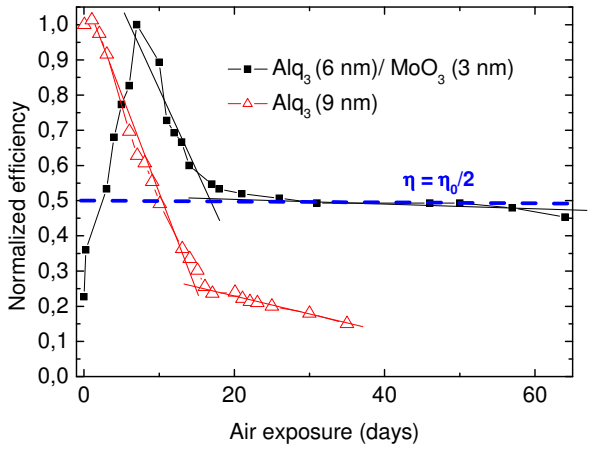

Fig. 3 — Variation with time of the normalized efficiency of OPVCs with different CBL: (■) Alq_3 (6 nm)/MoO_3 (3 nm) and (●) Alq_3 (9 nm)

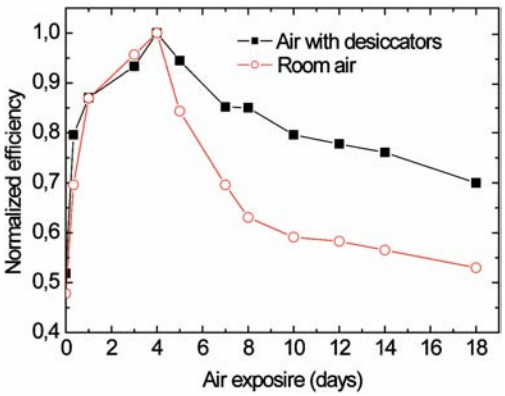

Fig. 4 — Variation with time of the normalized efficiency of OPVCs stored in different experimental conditions: (○): Stored in room air, (■): stored in the presence of a desiccators

used, the lifetime differences are clearly related to the specific properties of the various CBLs.

When kept in room air, device performance systematically decreases, at least after one week of air exposure in the case of OPVC with MoO_3 in their CBL, whereas, when kept in vacuum to rule out the effect of oxygen and water, the devices show very long lifetime.

In order to clarify the cause of degradation, we undertook studies under different atmospheric conditions. Some samples were placed in closed box with desiccators inside, which resulted in 25% humidity, while others were kept in room air where the humidity was 60%. By comparing the evolution of the performances of OPVCs in presence, or not, of desiccators, we can discriminate between humidity and oxygen contamination. We can see in Fig. 4 that, in the presence of a desiccators, the initial fast decrease period has nearly disappeared, which results in a curve more or less parallel to that corresponding to the slow degradation process visible in Fig. 3. It demonstrates the significant impact of humidity on the stability of the OPVCs. OPVC exposed to 60% relative humidity shows faster decay as compared to the OPVC exposed to 25% relative humidity. It means that the initial fast decrease of the efficiency is mainly due to water vapour contamination, while the slow degradation process corresponds to oxygen contamination of organic material. Since the degradation rate of this second process is far smaller when MoO_3 is present in the CBL, it means that MoO_3 is more efficient in limiting oxygen diffusion than water diffusion. From these experiments, the degradation can be attributed to a water/oxygen induced, mechanism.

4 Theory and Discussion

The presence or not of MoO_3 in the CBL of the OPVCs modifies strongly their ageing process. An equivalent circuit model could be helpful in understanding of the evolution of the OPVCs behaviour by providing a quantitative estimation for losses in the cells[20]. The equivalent circuit commonly used to interpret the I-V characteristics of solar cells

consists of a photogenerator connected in parallel with a diode, which represents the I–V characteristics in the dark. This corresponds to an ideal model in the absence of parasitic resistances. However, for modeling a real organic solar cell, a series resistance, R_s, and a shunt resistance, R_{sh} must be introduced to the equivalent circuit [Fig. 5(a)]. The mathematical description of this circuit is given by the following equation:

$$I = I_0\left[\exp\left(\frac{V - I\times R_s}{nkT}\right) - 1\right] + \frac{V - I\times R_s}{R_{sh}} - I_{ph} \quad \ldots (1)$$

where n is the ideality factor of the diode and I_{ph} the photo-generated current.

The electrical parameters, R_s, R_{sh}, n and I_{ph} can be determined using the Lambert W function, which is defined as the solution of the equation:

$$W(x).\exp[W(x)] = x.$$

The problem to be solved is the evaluation of a set of five parameters R_s, R_{sh}, n, I_{ph} and I_s in order to fit a given experimental I-V characteristics using a simple diode circuit. The resistance values under illumination are the more interesting values for solar cell characterisation and they will be determined carefully. For some OPVCs characteristics, it is impossible to achieve a good agreement between experimental and theoretical results, whatever the series and shunt resistance proposed. It shows that the simple equivalent circuit of Fig. 5(a) cannot explain these experimental results. In OPVCs, the process of carrier collection is one of the factors which controls the electrical characteristics and the efficiency of the devices. Therefore, any interface modification can lead to significant variation of the OPVCs performances. Indeed, the carrier collection depends in the barrier height at the interfaces, which, in a first approximation, is equal, in the case of the cathode contact, to the energy difference between the electrode work function Φelec and the Lowest Unoccupied Molecular orbital of the electron acceptor (EA) ($LUMO_{EA}$). When these values are different, there is a barrier at the interface, which induces the formation of a depletion layer. It was shown that the presence of a contact barrier can be modelled by introducing a second diode of opposite polarity[20,21]. Hence, it is assumed the presence of barrier at the interface EA/cathode [Fig. 5(b)]. If we assume a thermoionic current at this interface, the carrier current is:

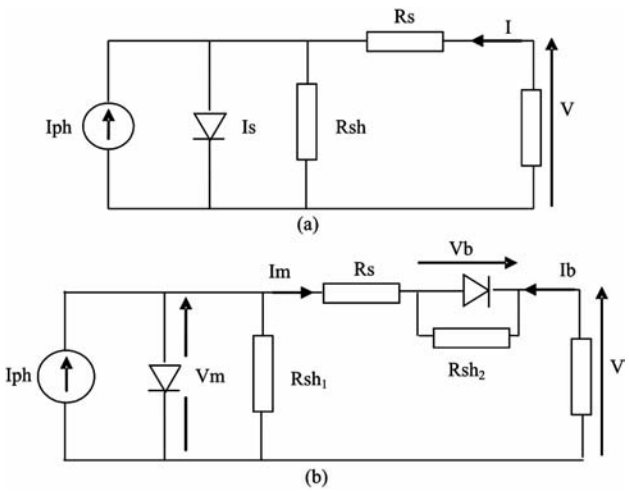

Fig. 5 — Equivalent electric circuit of (a) solar cell with ohmic contacts and (b) solar cell with rectifying back-contact

$$I_b = -I_{b0}\,(\exp(-qV_b/kT) - 1), \quad \ldots(2)$$

with I_{b0} the saturation current, V_b the voltage across the back contact, k Boltzmann constant, and T is the temperature. The current is negative because the polarity of the C_{60}/cathode junction is opposite to the main CuPc/C_{60} junction. Therefore, a current-limiting effect is expected from this parasitic junction and a S-shaped effect may occur because the total current saturate[21] at a value J_{b0}. The value of J_{b0} is the current value where the J–V curve starts to show rollover.

When a forward bias V is applied to the circuit, the voltage is divided between V_m across the main CuPc/C_{60} junction, V_b across the back-junction TCO/CuPc and IRs across the series resistance:

$$V = V_m + V_b + IR_s$$

Under illumination, the current across the main junction is:

$$I_m = I_{m0}\,(\exp(qV_m/nkT) - 1) - I_{ph} + Vm/R_{sh} \quad \ldots(3)$$

and through the back contact it is:

$$I_b = -I_{b0}\,(\exp(-qV_b/kT) - 1) + V_b/R^b_{sh} \quad \ldots(4)$$

Equating Eqs (3) and (4):

$$I_{m0}\,(\exp(qV_m/nkT) - 1) - I_{ph} + V_m/R_{sh} + I_{b0}\,(\exp(-qV_b/kT) - 1) - V_b/R^b_{sh} = 0 \quad \ldots(5)$$

The parameters R_s and I_{m0}, n, R_{sh} of the main diode are calculated in the region far from the saturation current I_b. As said above, I_{b0} is the current value where the J-V curve starts to show rollover. Then Eq. (5) can be solved. The above circuit models were used in order to achieve a good fitting between the experimental and theoretical J-V characteristics of the OPVCs studied.

So as to explain the reasons of the OPVCs characteristics evolution, we selected most significant J-V characteristics, among the ones measured in the whole interval days studied for each OPVC, as presented in Figs 6 and 7. Whatever the type of OPVC, it is evident that the shape of the curves varies with the time of air exposure. An inflexion point, giving a S-shaped curve, is often visible. As a consequence of the S-shaped curve, the FF is significantly reduced, which in turn reduces the performances of the OPVCs as well. Firstly, in the case of the OPVC with MoO_3 in the CBL, the S-shaped effect decreases progressively when the time of air exposure increases, until it disappears completely. Then, it reappears and gradually amplifies. In the case of reference OPVC, the S-shaped effect is absent at the beginning of the air exposure, while it appears progressively when the duration of the exposure increases

We can see in Figs 6 and 7 and in Tables 2 and 3 that the classical electrical equivalent scheme of Fig. 5(a) allows achieving a good agreement between

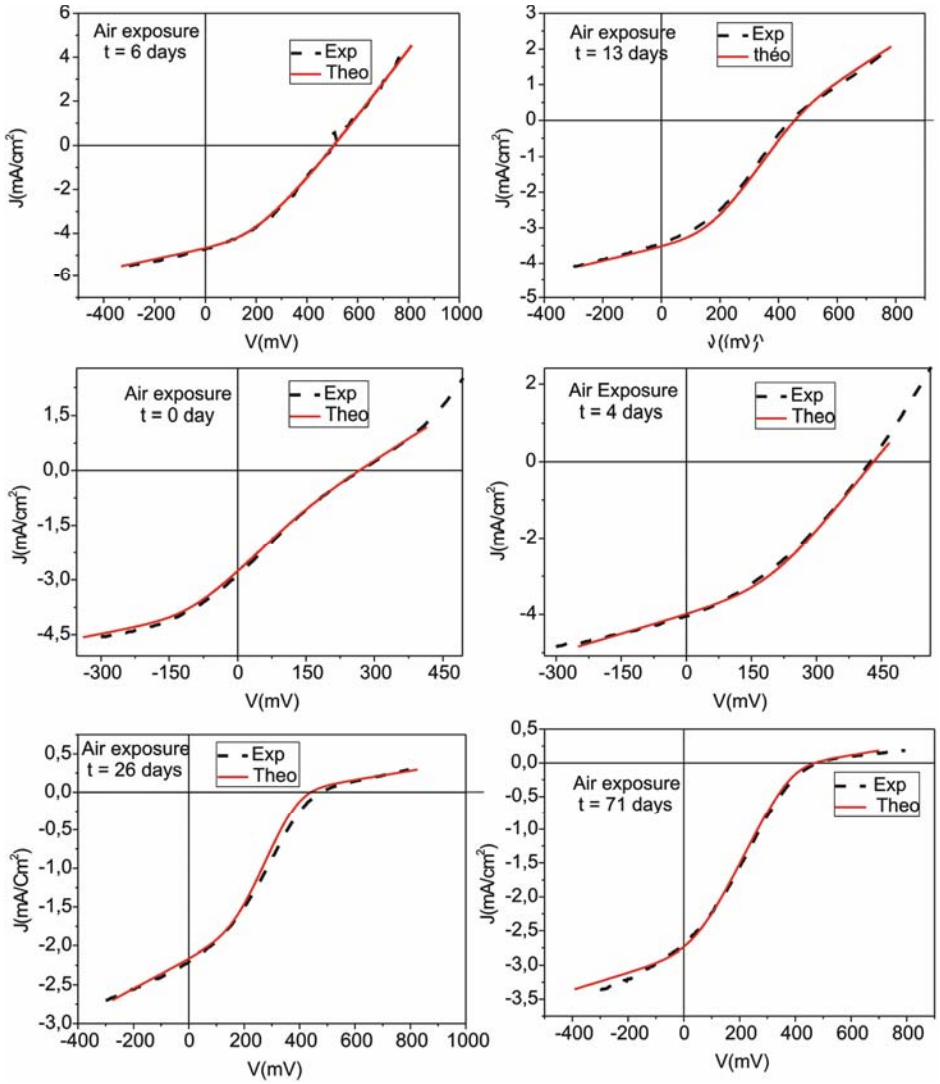

Fig. 6 — I-V characteristics under AM1.5 illumination of a solar cell using Alq_3 (6 nm)/MoO_3 (3 nm) as CBL for different duration of air exposure, (----) experimental and (____) theoretical curves

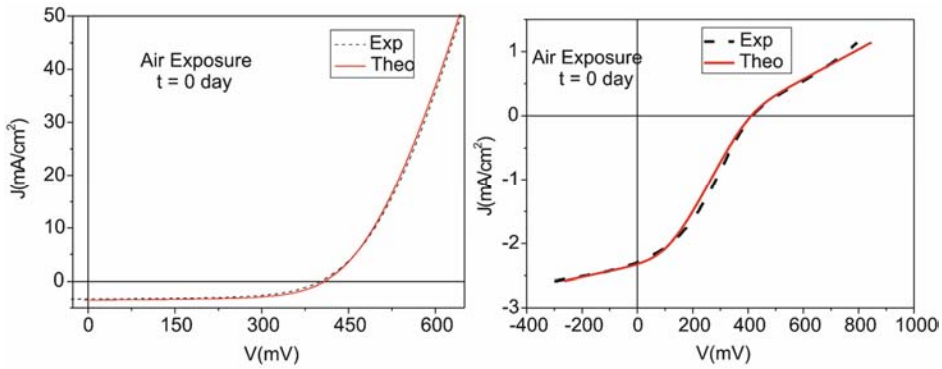

Fig. 7 — I-V characteristics under AM1.5 illumination of a solar cell using Alq_3 (9 nm) as CBL for different duration of air exposure, (----) experimental and (____) theoretical curves.

Table 2 — Variation with time of the calculated parameters for the OPVCs using Alq_3 (6 nm)/MoO_3 (3 nm) as CBL

	Diode 1					Diode 2			
	J_{ph} (mA/cm2)	J_{s1} (mA/cm2)	R_{s1} (Ω)	R_{sh1} (Ω)	n_1	J_{s2} (mA/cm2)	R_{s2} (Ω)	R_{sh2} (Ω)	n_2
0 Day	4.57	7×10^{-4}	35	360	1.2	4.2×10^{-2}	15	70	1.0
6 hours	4.55	2.5×10^{-3}	20	350	1.6	1.2×10^{-1}	20	50	1.3
4 Days	4.82	9×10^{-5}	20	250	1.6	8×10^{-1}	20	40	1.3
6 Days	5.50	4×10^{-5}	60	349	1.7		/	/	/
13 Days	4.07	5×10^{-5}	30	450	1.6	5×10^{-1}	20	130	1.3
18 Days	3.60	7×10^{-6}	33	450	1.4	9×10^{-2}	24	400	1.3
26 Days	2.70	9×10^{-6}	33	450	1.4	7×10^{-2}	24	1600	1.3
31 Days	3.63	6×10^{-5}	30	500	1.7	4×10^{-2}	20	1100	1.3
50 Days	3.90	4×10^{-5}	35	650	1.6	4×10^{-2}	42	1600	1.3
71 Days	3.35	6×10^{-5}	40	720	1.7	3×10^{-2}	30	1500	1.3
85 Days	3.03	9×10^{-5}	40	420	1.8	3×10^{-2}	2	1600	1.2

Table 3 — Variation with time of the calculated parameters for the OPVCs using Alq_3 (9 nm) as CBL

Number of days	Diode 1					Diode 2			
	J_{ph} (mA/cm2)	J_{s1} (mA/cm2)	R_{s1} (Ω)	R_{sh1} (Ω)	n_1	J_{s2} (mA/cm2)	R_{s2} (Ω)	R_{sh2} (Ω)	n_2
0	3.528	$2.7\ 10^{-4}$	2.2	1020	1.7				
6	3.015	$2.0\ 10^{-4}$	12	1020	1.8	$5.0\ 10^{-4}$	20	40	1.2
10	2.580	$2.5\ 10^{-5}$	50	1020	1.4	$1.7\ 10^{-4}$	20	350	1.2
15	2.091	$2.5\ 10^{-4}$	45	1080	1.5	$2.5\ 10^{-4}$	30	1050	1.2

the experimental and theoretical fit only when the OPVCs exhibit their better performances. In other cases, i.e., when the S-shaped effect is visible, it is necessary to use the electrical equivalent scheme of Fig. 5(b), that is to say, two diodes, with one in opposite direction, are necessary to reflect the shape of the curves.

Firstly, in the case of OPVCs with MoO_3 in its CBL, an S-shaped curve is obtained immediately after air exposure, and then, it progressively disappears during the first 5-6 days. The S-shaped effect is due to the presence of MoO_3 in the CBL since it is not present in the case of reference OPVCs.The formation of this barrier can be explained by the high work function of MoO_3. Now, it is well accepted that, after deposition under ultra high vacuum by sublimation, the work function[10] of MoO_3 is 6.9 eV, while it is around 6.2 eV in classical vacuum[22] (10^{-4}Pa). With this Wf value, the band structure of the interface is such that at the $C_{60}/Alq_3/MoO_3/Al$ interface, the passage of holes is easier than that of electrons[10] (Fig. 8). On the other hand, it was also shown that air

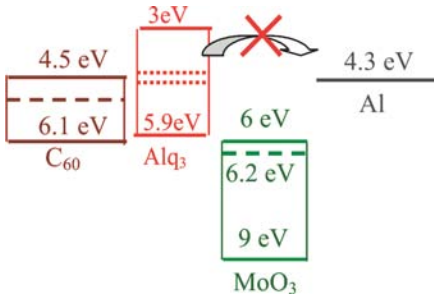

Fig. 8 — Band scheme of the interface $C_{60}/Alq_3/MoO_3/Al$ just after deposition.

exposure of MoO_3 induces a progressive Wf decrease[22] of around 1 eV. In our case, using a Kelvin probe, we found that the work function of our MoO_3 thin films is 5.1 eV after air exposure [see Table 2 in Ref 23], which decreases the electron barrier at the interface and facilitates electrons transfer.

Therefore, the evolution of the J-V characteristics of the OPVCs with the duration of air exposure corresponds to a progressive air contamination of the OPVCs. The first layer encountered by the diffused contaminant after crossing the Al polycrystalline film is the MoO_3 layer. Due to this progressive contamination, the Wf of MoO_3 will decrease gradually until it reaches its minimal value of 5.1 eV. In parallel the height of the barrier present at the interface C_{60}/cathode decreases, which justifies the progressive improvement, during the first 6 days of air exposure, of the OPVCs efficiency [Fig. 6 (a-c)]. Then, after the maximum efficiency is reached, whatever the kind of OPVC, there is a progressive degradation of the performance which corresponds to the (re)appearance of the S-shaped effect. It means that, during the fast decay, whatever the CBL of the OPVC, the electrical equivalent scheme needs changes from the classical one diode equivalent electrical scheme [Fig. 5(a)] to the equivalent electrical scheme with two diodes as shown in Fig. 5(b), which means that there is interface properties modification with, diode formation at the interface C_{60}/CBL/Al.

Some hypothesis can be proposed to explain the variation with time of the contact C_{60}/CBL/Al. Due to air exposure, the contamination reaches the C_{60} layer and the OPVCs performances decrease. It is known that the oxygen/water contamination of C_{60} increases its resistivity[24]. It must be noted that this degradation occurs very quickly for conventional cells, whereas several days are needed before it is sensitive in the presence of MoO_3. The S-shaped J-V characteristics indicate a formation of a barrier at the interface C_{60}/cathode. Actually, the formed traps in the C_{60} layer by H_2O/oxygen absorption might establish a space charge, which induces a diode formation and would decrease Jsc and FF. The reduced current (Tables 2 and 3) results from an increase of the energy barrier at the interface. In the present work, C_{60} is deposited on the top of CuPc layer and thus the C_{60} layer is the first one to be attacked by water and oxygen, both of which could dramatically deteriorate the electrical transportability of the C_{60} layer, resulting in an increase of the series resistance and a reduction[25] of FF. The S-shape behaviour can be explained by imbalanced profiles of charge carrier densities and field distribution within the layers. Presently, this charge accumulation at the interface cathode/C_{60} must be due to resistive[26,27] C_{60}.

The lifetime of the OPVCs with MoO_3 in their CBL is far higher. Since the structure of all the devices is the same except different buffer layers are used, the lifetime variation can be attributed to the specific properties of the different CBL. With MoO_3 in the CBL, the lifetime improvement results probably from the reason that it effectively blocks, at least partly, the oxygen and/or water to permeate through the acceptor layer. After the first step of fast decrease of the OPVC efficiency, the behaviour of the cells is clearly different. In the case of the reference cells, the change of the slope of the curve operates only for $\eta = 0.35\ \eta_0$, while it operate for $\eta = 0.55\ \eta_0$ for cells with MoO_3 in their CBL.

If, in the presence of MoO_3 in the CBL, the lifetime is improved, a clear degradation process stays visible, which means that some air diffusion, even if strongly decreased, stays present in the structures, mainly during the initial fast decrease. The discussion above shows that, in room air, the degradation of the OPVCs is controlled by two processes. By only reducing the room humidity of the store environment, the fast decay disappears nearly totally (Fig. 4). Thus, it is reasonable to ascribe the fast decay mainly to the water and the slow one to the oxygen. It has been demonstrated that water is more detrimental than oxygen in the transport of organic semiconductors[28]. Moreover, it was shown that water diffusion seems to determine the degradation rate of OPVCs, which can justifies this initial degradation process[29]. It may also means that MoO_3 is less efficient in trapping water than oxygen. Then, the slow decay can be attributed to

the bulk effect related to progressive C_{60} contamination with oxygen.

The big lifetime difference between the two OPVCs families could be explained by the effect that the double CBL, Alq_3/MoO_3, has on the organic material contamination. On one hand, it is already known that the stability of the OPVCs with Alq_3 as CBL is higher than that with BCP. It has been attributed to the stability of the amorphicity of Alq_3 while BCP tends to crystallize, which facilitates contamination diffusion towards the underlayers of the cells[30]. Actually, grain boundaries in the layers act as a short circuit pathway for diffusion.

It is known that gas transport through polycrystalline thin films takes place at grain boundaries. In the present work, Alq_3 and MoO_3 are amorphous, which does not exclude layer defects, especially since the layers are very thin. So, even if the films are amorphous, gas diffusion will take place at pinholes present in the films [Fig. 9(a)], the solid state diffusion being several orders of magnitude lower and therefore, is negligible. A possibility to circumvent this diffusion is to use a combination of at least two barrier layers. Changing the nature of the barrier layer interrupts the growth of defects and increases the path of permeating gas [Fig. 9(b)]. This results in an increase of the lag-time of the permeation[31] and therefore of the lifetime of the OPVCs. About the higher efficiency of the CBL with MoO_3 in front of oxygen than in front of water, it was proposed that, inside the device, oxygen diffusion is much slower than the diffusion of water due to the difference in size[32]. The CBL being composed of two amorphous layers, which exclude the presence of grain boundary, while it increases the diffusion path will decrease the diffusion rate of all contaminate, but with more efficiency for the bigger contaminant, here oxygen. On the other hand, F. Jin *et al*[12]. attribute the MoO_3 effect to the fact that it is a stable inorganic material and it prevents organic material from Al diffusion. These two hypotheses are not mutually exclusive but rather they can contribute simultaneously to the effect of MoO_3.

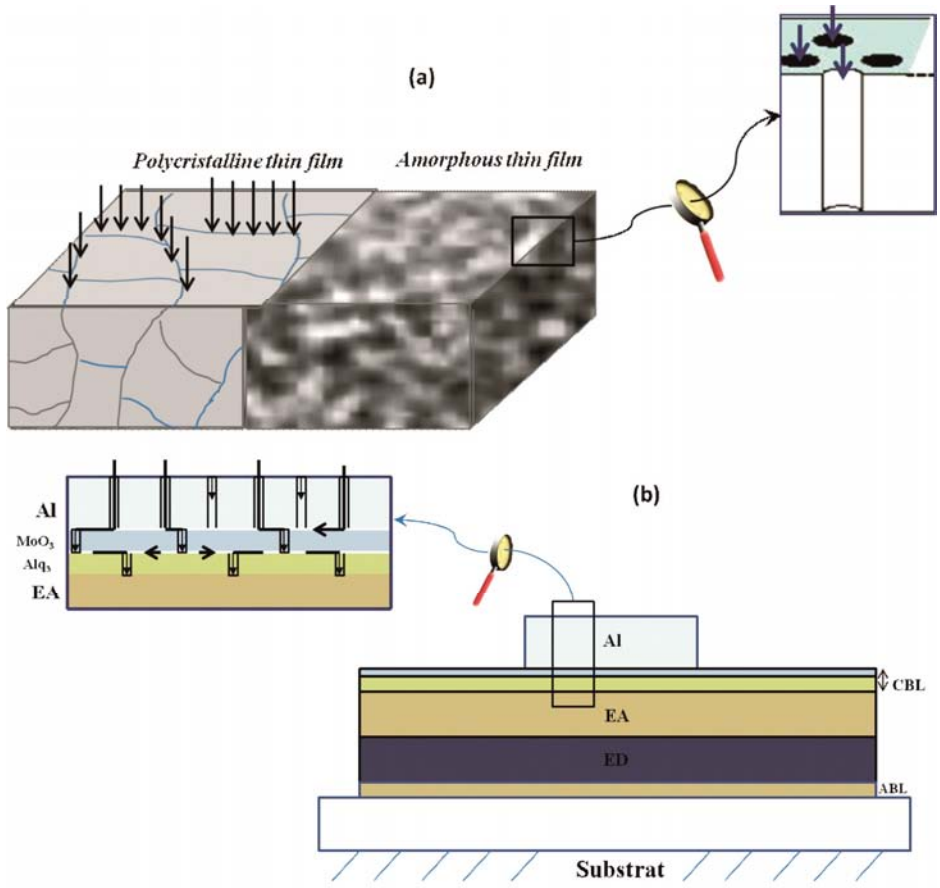

Fig. 9 — (a) Mapping of diffusion paths in polycrystalline and amorphous layers and (b) Multilayer barrier structure consisting of Alq_3/MoO_3 amorphous layers

6 Conclusions

We show that, if just after deposition the introduction of a MoO_3 layer in the CBL does not allow improving the OPVC efficiency, it improved strongly its lifetime.

This discrepancy, about the initial efficiency of the OPVCs, between our results and those of the Refs (11 and 12) may be attributed to the facility of Wf to vary with the history of the MoO_3 layer. Indeed, the films used by Vasilopoulou *et al* [11]. are strongly oxygen deficient, which induces a significant decrease of Wf of MoO_3 and an acceptable band matching.

We show through experimental studies that the initial variation of the performances of OPVCs with MoO_3 in their CBL is due to the variation of the value of MoO_3 Wf. Then, by comparing the results of the different devices, it is evident that the presence of MoO_3 in the CBL is beneficial to the lifetime of the OPVCs. The degradation curves of the efficiency of the OPVCs exhibit two different regimes, a fast decrease followed by a slower one. The fast decrease is shown to be due to water contamination of the organic layers, while the slow subsequent decrease is due to oxygen contamination. The enhancement of the OPVCs lifetime in presence of MoO_3 in the CBL is due to the fact that MoO_3 is amorphous and to the well known effect of using two protecting layers.

Acknowledgement

This work has been financially supported by the Hassan II Academy of Science and Technology (Morocco).

References

1 Cai W, Gong X & Cao Y, *Sol Energy Mater Sol Cells*, 94 (2010) 114.
2 You J, Dou I, Yoshimura K, Kato T, Ohya K, Moriarty T, Emery K, Chen C-C, J Gao, Li C & Yang Y, *Nat Commun*, 4 (2013) 1446.
3 Gevorgyan S A, Medford A J, Bundgaard E, Sapkota S B, Schleiermacher H-F, Zimmermann B, Würfel U, Chafiq A, Lira-Cantu M, Swonke T, Wagner M, Brabec C J, Haillant O, Voroshazi E, Aernouts T, Steim R, Hauch J A, Elschner A,Pannone M, Xiao M, Langzettel A, Laird D, Lloyd M T, Rath T, Maier E, Trimmel G, Hermenau M, Menke T, Leo K, Rösch R, Seeland M, Hoppe H, Nagle T J, Burke K B, Fell C J, Vak D, Singh Th B, Watkins S E, Galagan Y, Manor A, Katz E A, Kim T, Kim K, Sommeling P M, Verhees W J H, Veenstra S C, Riede M, Christoforo M G, Currier T, Shrotriya V, Schwartz G & Krebs F C, *Sol Energy Materials & Sol Cells,* 95 (2011) 1398.
4 Bundgaard E & Krebs F C, *Sol Energy Mater Sol Cells*, 91 (2007) 954.
5 Krebs F C, *Organic Electronics*, 10 (2009) 761.
6 Jorgebsen M, Norrman K & Krebs F C, *Sol Energy Mater Sol Cells*, 92 (2008) 686.
7 Rand B P, Li J, Xue J, R Holmes J, Thompson M E & Forrest S R, *Adv Mater*, 17 (2005) 2714.
8 Norman K, Madsen M V, Gevorgyan S A & Krebs F C, *J Am Chem Soc*, 132 (2010) 16883.
9 Makha M, Cattin L, Dabos-Seignon S, Arca E, Velez J, Stephant N, Morsli M, Addou M & Bernède J C, *Indian J of Pure & Appl Phys*, 51 (2013) 569.
10 Meyer J, Hamwi S, Kröger M, Kowalsky W, Riedl T & Kahn A, *Adv Mater*, 24 (2012) 5408.
11 Vasilopoulou M, Palilis L C, Georgiadou D G, Argitis P, Kennou S, Sygeliou L, Kostis I, Papadimitropoulos G, Konofaos N, Liadis A A & Davazoglou D, *Appl Phys Lett*, 98 (2011) 123301.
12 Jin F, Chu B, Li W, Su Z, Zhao B, Yan X, Zhang F, Fan D, Zhang T, Gao Y, Lee C S & Wang J, *Sol Energy Mater & Sol Cells*, 117 (2013) 189.
13 Cattin L, Dahou F, Lare Y, Morsli M, Tricot R, Houari S, Mokrani A, Jondo K, Khelil A, Napo K & Bernède J C, *J App Phys*, 105 (2009) 034507.
14 Vivo P, Jukola J, Ojala M, Chukharev V & Lemmetyinen H, *Sol Energy Mater Sol Cells*, 92 (2008) 1416.
15 Lare Y, Kouskoussa B, Benchouk K, Djobo S Ouro, Cattin L, Morsli M, Diaz F R, Gacitua M, Abachi T, delValle M A, Armijo F, East G A & Bernède J C, *J of Phys & Chem of Solids*, 72 (2011) 97.
16 Berredjem Y, Karst N, Boulmokh A, Gheid A H, Drici A & Bernède J C, *European Phys J Appl Phys*, 40 (2007) 163.
17 Latef A & Bernède J C, *Phys Stat Sol*, 124 (1991) 243.
18 Ouerfelli J, Djobob S Ouro, Bernède J C, Cattin L, Morsli M & Berredjem Y, *Materials Chem & Phys*, 112 (2008) 198.
19 Jorgensen M, Norrman K & Krebs F C, *Sol Energy Mater Sol Cells*, 92 (2008) 686.
20 B Kouskoussa, M Morsli, K Benchouk, G Louarn, L Cattin, A Khelil & Bernède J C, *Physica Status Solidi*, 206 (2009) 311.
21 Demtsu S H & Sites J R, *Thin Solid Films*, 510 (2006) 320.
22 Irfan I, Ding H, Gao Y, Small C, Kim D Y, Subbiah J & So F, *Appl Phys Lett*, 96, (2010) 243307.
23 Bernède J C, Cattin L, Makha M, Jeux V, Leriche P, Roncali J, Froger V, Morsli M & Addou M, *Sol Energy Materials & Sol Cells*, 110 (2013) 107.
24 Hamed A, Sun Y Y, Tao Y K, Meng R L & Hor P H, *Phys Rev B*, 47 (1993) 10873.
25 Vivo P, Jukola J, Ojala M, Chukharev V & Lemetyninen H, *Sol Energy Mater Sol Cells*, 92 (2008) 1416.
26 Kulshreshtha C C, Choi J W, Kim J-K, Jeon W S, Suh M C, Park Y & Kwon J H, *Appl Phys Lett*, 99 (2011) 023308.
27 Wang J C, Ren X C, Shi S Q, Leung C W & Chan P K L, *Organic Electronics*, 12 (2011) 880.
28 Yang H B, Song Q L, Gong C & Li C M, *Sol Energy Mater Sol Cells*, 94 (2010) 845.
29 Nikiforov M P, Strzalka J & Darling S B, *Sol Energy Mater Sol Cells*, 110 (2013) 36.
30 Song Q L & Li F Y, *Chem Phys Lett*, 416 (2005) 42.
31 Fahlteich J, Fahland M, Schönberger W & Schiller N, *Thins Solid Films*, 517 (2009) 3075.
32 Klumbies H, Karl M, Hermenau M, Rösch R, Seeland M, Hoppe H, Müller-Meskamp L & Leo K, *Sol Energy Mater Sol Cells*, 120 (2014) 685.